remote sensing

MDPI

Article

Spatio-Temporal Variability of Wind Energy in the Caspian Sea: An Ecosystem Service Modeling Approach

Milad Rahimi [1], Mehdi Gholamalifard [1,*], Akbar Rashidi [2], Bonyad Ahmadi [1], Andrey G. Kostianoy [3,4] and Aleksander V. Semenov [4]

[1] Department of Environment, Faculty of Natural Resources & Marine Sciences (FNRMS), Tarbiat Modares University (TMU), Noor 46414 356, Mazandaran, Iran
[2] Department of Marine Physics, Faculty of Natural Resources & Marine Sciences (FNRMS), Tarbiat Modares University (TMU), Noor 46414 356, Mazandaran, Iran
[3] P.P. Shirshov Institute of Oceanology, Russian Academy of Sciences, Nakhimovsky pr. 36, 117997 Moscow, Russia
[4] Laboratory of Integrated Research of Water Resources, S.Yu. Witte Moscow University, Second Kozhukhovsky pr. 12, Build. 1, 115432 Moscow, Russia
* Correspondence: m.gholamalifard@modares.ac.ir; Tel.: +98-11-4499-8107

Abstract: The ecosystem services that can be obtained from the oceans and seas are very diverse; one of the sources of energy is wind power. The Caspian Sea is characterized by a fragile ecosystem that is under serious anthropogenic stress, including oil and gas production and transportation. In particular, rich oil and gas resources in the region make renewables less important for the Caspian Sea Region. Depletion of hydrocarbon resources, a rise of their price on the international markets, geopolitical tensions, a decrease in the Caspian Sea level, regional climate change, and other factors make exploring offshore wind energy production timely. In order to model the offshore wind energy of the Caspian Sea, data from the ERA-Interim atmospheric reanalysis were used from 1980 to 2015 combined with QuikSCAT and RapidSCAT remote sensing data. The modeling results showed a wind power density of 173 W/m^2 as an average value for the Caspian Sea. For the 1980–2015 period, 57% of the Caspian Sea area shows a decreasing trend in wind power density, with a total insignificant drop of 16.85 W/m^2. The highest negative rate of change is observed in the Northern Caspian, which seems to be more influenced by regional climate change. The Caspian Sea regions with the highest potential for offshore wind energy production are identified and discussed.

Keywords: offshore wind energy; QuikSCAT; RapidSCAT; Caspian Sea; ecosystem services

Citation: Rahimi, M.; Gholamalifard, M.; Rashidi, A.; Ahmadi, B.; Kostianoy, A.G.; Semenov, A.V. Spatio-Temporal Variability of Wind Energy in the Caspian Sea: An Ecosystem Service Modeling Approach. *Remote Sens.* **2022**, *14*, 6263. https://doi.org/10.3390/rs14246263

Academic Editors: Bryan Stiles, Svetla Hristova-Veleva, Lucrezia Ricciardulli, Larry O'Neill, Zorana Jelenak and Joe Sapp

Received: 7 October 2022
Accepted: 7 December 2022
Published: 10 December 2022

1. Introduction

Today, food, freshwater, and energy are considered as the main factors in the well-being of a society. In the last three decades, energy consumption globally has increased three and a half times [1]. Electricity is one of the most important energy resources. Population growth, expansion of cities, industry, roads, infrastructure, and arable lands on the limited terrestrial spaces today have brought more attention to marine ecosystem services and sea and ocean goods [1–4]. Recreation, tourism, maritime transport, and offshore wind generation are familiar services provided by many marine ecosystems.

The Global Wind Report 2022 [5] shows the fast-growing offshore wind sector, with an additional 94 GW of wind installed in 2021 around the world, from which 21 GW is offshore. The 94 GW of new installations in 2021 brings global cumulative wind power capacity to 837 GW, showing year-to-year growth of 12% [5]. The onshore wind market added 72.5 GW worldwide due to the largest wind markets in the USA and China, as well as due to the record-high growth in Europe (+19%), Latin America (+27%), and Africa and the Middle East (+120%). The offshore wind market in 2021 added 21.1 GW, which is three times more than the previous year. New offshore installations represented 22.5%

of all new installations last year, which bring the world's total offshore capacity to 57 GW, which is 7% of global installations. China contributed 80% of that offshore growth. In Vietnam, 779 MW of nearshore projects were commissioned, making it the third-largest market for offshore installations in 2021. In Europe, the UK is a leader in new offshore installations, with 2.3 GW added to the grid [5]. The UK, Germany, Denmark, Italy, Spain, and Poland are among the most active countries in the field of onshore and offshore wind energy generation [5]. Offshore wind brought Europe to 18.1 GW in 2021, but it is not a high enough volume, considering that the EU needs 32 GW of new wind capacity each year until 2030 to reach its carbon neutrality target by 2050. One of the main obstacles to wind-generation development in Europe and the world in 2020–2021 was the COVID-19 pandemic [5].

The correct identification and evaluation of the spatial distribution of energy potential for offshore wind generation are of vital importance to reduce uncertainties in wind farm construction [6]. Today, there are various data sources and methods for calculating wind energy potential using remote sensing data, numerical models (atmospheric reanalysis), and weather station records [7–14]. Wind, as the key factor in the development of wind farms, has several important characteristics such as speed and direction that should be known at different heights of the boundary layer [6]. The authors of [12] evaluated the sensitivity of wind power to height over the ice-free global oceans for 2000–2006 and showed that the global mean wind power at 100 m height (776 W m^{-2}) is 1.6 times larger than at 10 m (487 W m^{-2}). Due to increased wind shear in the boundary layer and the cubic dependence of wind power on speed, frequent high-wind-speed regions have the greatest increase in power with height. Thus, the storm track regions experience the greatest increase in annual mean wind power with height. For example, for 2000–2006 a 100 m hub-height wind turbine could capture 69% (74%) more power within the Northern (Southern) Hemisphere storm track than at 10 m height [12]. They also showed that wind power at 80 m height accumulates at a rate of 20–45 MW km^2 m^{-2} per meter depth increase from the shore to the shelf break. Beyond the shelf break, wind power accumulates at a slower rate (<12 MW $km^2m^{-2}m^{-1}$) [12]. This effect should also be taken into account when evaluating wind power potential and planning wind farm construction. Seasonal and interannual variability of wind speed, including climate-related changes, should be well identified to ensure future cost-effective wind energy production. This is especially important for offshore wind farms, where the cost of energy generation and maintenance is higher than for onshore wind farms [7–9].

As concerns the Black, Azov, and Caspian seas, there are many investigations on wind and wave characteristics [15–26], but it is little known about wind energy generation potential in these water areas [26–34]. For the Caspian Sea, the authors of [33] conducted an evaluation of the wind energy potential based on the NCEP-CFSR (Climate Forecast System Reanalysis) dataset at 12 locations for 1999–2008. Seasonal and spatial variations of wind speed and power density were significant. The highest values of power density of up to 300 W m^{-2} for the total time and up to 426 W m^{-2} for wintertime were obtained for the coastal zone of Kazakhstan between Fort-Shevchenko and Aktau (see points C5 and C6, respectively) in the northern part of the Middle Caspian Sea. Points C9 and C10, located along the coast of Iran, showed the lowest power density—less than 30 W m^{-2}. A recent study by [34] mapped the Southern Caspian potentials for wind and wave energy using ECMWF numerical model data for 2009–2015. In this study, 100 different points were used for calculations, which showed the power density in the Southern Caspian to be less than 100 W/m^2.

The objective of this study is to assess the spatiotemporal variability of available wind resources for wind farm construction in the whole area of the Caspian Sea based on the ERA-Interim global atmospheric reanalysis from 1980 to 2015 combined with the QuikSCAT and RapidSCAT remote sensing data. These data were used to calculate wind energy and wind power changes in the basin. The Caspian Sea locations that are most favorable for wind energy production are identified and discussed. Capps and Zender [12] showed

that a combination of the QuikSCAT remote sensing and atmospheric reanalysis data is an effective tool for investigation of wind power potential.

2. Data and Methods

2.1. Study Area

The Caspian Sea is the world's largest closed sea basin, with its own specific geographical, meteorological, oceanographic, climatic, ecological, and political significance. The coastline of the five Caspian Sea countries—Iran, Azerbaijan, Russia, Kazakhstan, and Turkmenistan—is 7000 km long. The sea is 1030 km long and 320 km wide on average. In terms of bottom topography, the sea is divided into three regions (Figure 1): the Northern Caspian with depths less than 50 m (average depth of 5–6 m), the Middle Caspian with an average depth of 190 m, and the Southern Caspian (max depth of 1025 m), which is the deepest part of the Caspian Sea [17].

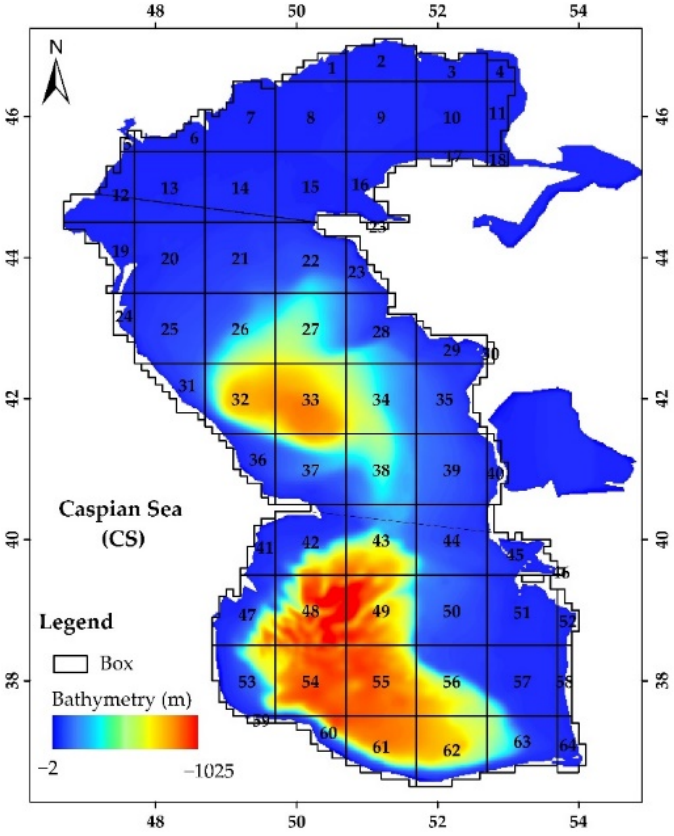

Figure 1. The Caspian Sea Bathymetry.

The length of the Caspian Sea determines very different climate and weather regimes, where the Northern Caspian freezes partially every winter and the Southern Caspian is the warmest part of the sea. The same is valid for other meteorological parameters and wind speed and direction, in particular because different parts of the Caspian Sea are subjected to different atmospheric forcing. Before 1991 (the Caspian Sea was divided between the USSR and Iran) the number of coastal weather stations in the USSR was over 70, then it was reduced dramatically [15,35]. Lebedev and Kostianoy [15] argued that in the conditions of the significant reduction in the number of weather stations in the Former Soviet Union countries, the absence of meteorological and oceanographic data exchange between countries and the significant decrease in scientific collaboration, the use of different kinds of satellite remote sensing data, and atmospheric and oceanic reanalyses, as well as numerical modeling are the alternatives to overcome the lack of in situ metocean data.

2.2. Data Lake

A series of previous publications has shown the efficiency of the use of combined remote sensing and atmospheric reanalysis data for the evaluation of wind power potential, namely for offshore wind energy generation due to the lack of in situ records [7–14,29,36,37]. In the present study, we also combine the QuikSCAT and RapidSCAT remote sensing data on wind speed with global atmospheric reanalysis ERA-Interim data on wind speed.

The primary mission of QuikSCAT (Quick Scatterometer), carrying the SeaWinds scatterometer, was to measure the surface wind speed and direction over the ice-free global oceans. It operated from 19 June 1999 to 2 October 2018. QuikSCAT provided measurements of the wind speed and direction referenced to 10 m above the sea surface at a spatial resolution of 25 km. Wind information cannot be retrieved within 15–30 km of coastlines or in the presence of sea ice. Measurements of wind speeds are available between 3–20 m/s to an accuracy of 2 m/s, wind vector directions—to an accuracy of 20° [38]. Wind speed data were taken from the following website: https://podaac.jpl.nasa.gov/datasetlist?search=quick (accessed on 6 October 2022) for the period from 1 January 2000 to 27 November 2009 (10,777 records).

The ISS-RapidSCAT was an instrument mounted to the International Space Station's "Columbus" module that measured global wind speed data from September 2014 to August 2016. The scatterometer was very similar to QuikSCAT in functionality. Wind speed data were taken from the following website: https://podaac.jpl.nasa.gov/datasetlist?ids=&values=&search=rapid&view=list&provider (accessed on 6 October 2022) for the period from 1 October 2014 to 30 December 2016 (3644 records).

Global atmospheric reanalysis ERA-Interim was used to obtain wind speed data with a spatial resolution of 0.75 degrees with a step of 6 h for the 36-year period from 1 January 1980 to 31 December 2015. The reanalysis was available from 1 January 1979 to 31 August 2019. It was superseded by the ERA5 reanalysis. The data assimilation system used to produce ERA-Interim is based on a 2006 release of the IFS (Cy31r2). The system includes a 4-dimensional variational analysis (4D-Var) with a 12 h analysis window. The spatial resolution of the dataset is approximately 80 km at 60 levels vertically from the surface up to 0.1 hPa [39]. Wind speed data were taken from the following website: https://apps.ecmwf.int/datasets/data/interim-full-daily/levtype=sfc/ (accessed on 6 October 2022) The accuracy of the ERA-Interim wind speed data is 1.10 m/s [40].

To assess the accuracy of the ERA-Interim wind speed data, we used QuikSCAT and ISS-RapidSCAT data, which showed a good correspondence (see Section 3.1). The accuracy of the wind speed computed by the model was evaluated through conventional statistical analysis [41] with the following Equation (1):

$$\begin{gathered} CC = \frac{\sum_{i=1}^{n}\left(X_i-\overline{X}\right)\left(Y_i-\overline{Y}\right)}{\sqrt{\sum_{i=1}^{n}\left(X_i-\overline{X}\right)^2}\sqrt{\sum_{i=1}^{n}\left(Y_i-\overline{Y}\right)^2}} \\ RMSE = \sqrt{\frac{\sum_{i=1}^{n}\left(Y_i-X_i\right)^2}{n}} \\ Bais = \overline{X} - \overline{Y} \end{gathered} \tag{1}$$

where CC is the correlation coefficient, $\overline{X}$ is the mean of QuikSCAT and RapidSCAT, X_i is the value of wind speed in i in the QuikSCAT and RapidSCAT, $\overline{Y}$ is the mean of ERA-Interim, Y_i is the value of wind speed in i in the ERA-Interim data, i.

2.3. Wind Power Density

An energy assessment for wind energy projects is based on spatial distribution of wind power density, which is one of the key parameters. Power density is also used in the design of the site and turbine blade. In order to calculate the amount of energy per unit area, the following equation for power density (PD) can be used [42]:

$$PD = \frac{1}{2}\,\rho \sum_{j=1}^{n}\left(f\,(v_j) \times {v_j}^3\right) \tag{2}$$

where PD is the concentration density in a given area in W m^{-2}, ρ is air density in kg/m^3, ν is wind speed, $f(v_j)$ is the probability of wind blowing at a specific speed.

One of the key factors in many computations is the air boundary layer. It is directly influenced by the earth's surface. However, other physical parameters such as acceleration, temperature, and humidity are subject to fluctuations in both space and time. Air density is an important factor of the boundary layer under the influence of temperature and pressure. To calculate the air density, we can use the ideal gas equation:

$$\rho = \frac{P}{RT} = 3.4837 \frac{P}{T} \quad (3)$$

where P is air pressure, T indicates air temperature in Kelvin, and R is the ideal gas constant, so air density is measured in kg/m^3.

Usually for modeling wind energy, various statistical functions such as the Weibull distribution [43] and Rayleigh distribution are used [44,45]. Numerous studies have been performed to assess the precision of these models, and in general, the Weibull function provides a more accurate result when compared to the data. For this reason, the Weibull function was used to model wind energy. The accuracy of these statistical functions depends on the type and accuracy of their parameters. There are several methods to calculate the parameters of these functions. The methods of standard deviation, moment probability, most probability of neighborhood, and energy distribution are usually used [6]. In wind turbine studies, the Weibull function has the highest application accuracy and Equation (4) represents the probability density function of Weibull:

$$f(v) = \frac{k}{\lambda} \left(\frac{v}{k}\right)^{k-1} e^{-\left(\frac{v}{k}\right)^k} \quad (4)$$

In the equation, k, λ represent the shape and scale parameters, respectively. Shape parameter is a dimensionless number [46], which is a way of showing the variability of wind speed. In fact, in the probability distribution plots, the function is impacted by the line of slope. In other words, the wind variability is reduced with the increase in the form parameter. The scale parameter, however, is represented in m/s [46]. The wind speed concentration in a certain range is really indicated by this parameter. The smallness of the scale factor helps to increase the probability of wind speed. In other words, modifications to this parameter have an impact on the distribution's scale value of the base curvature [47]. The values of v, f (v) represent the wind speed and the probability of the wind speed, respectively, and e is equal to the Neper number.

The scale parameter influences the probability distribution function while maintaining a constant shape parameter (2a). The parameter shape (β) has an impact on the probability distribution function, as seen in Figure 2B; for instance, the three Weibull parameters are reduced to two parameters with an exponential distribution when its value is one (β = 1). Although each of the five Weibull distributions in Figure 2B has a different Weibull k value, they all have an average wind velocity of about 9 m/s. Lower k values, as seen in the graph, correspond to greater ranges of wind velocity, indicating that winds often fluctuate over a wide range of velocity and vice versa.

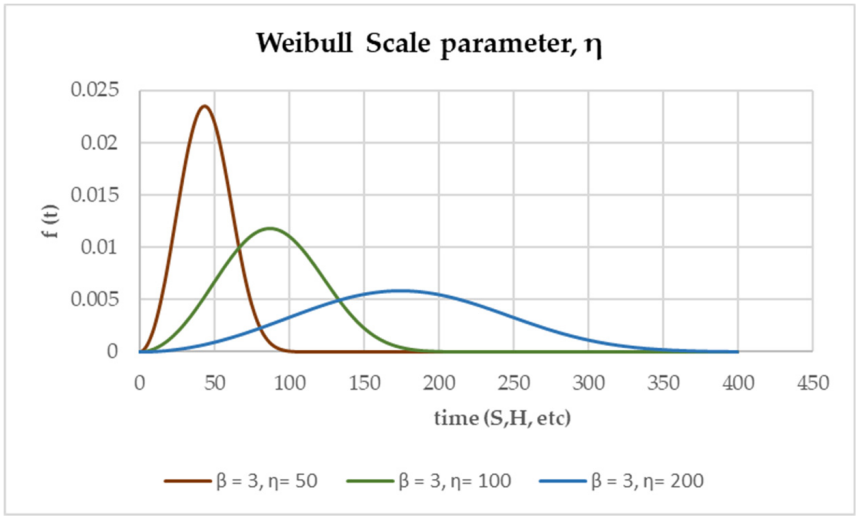

(**A**)

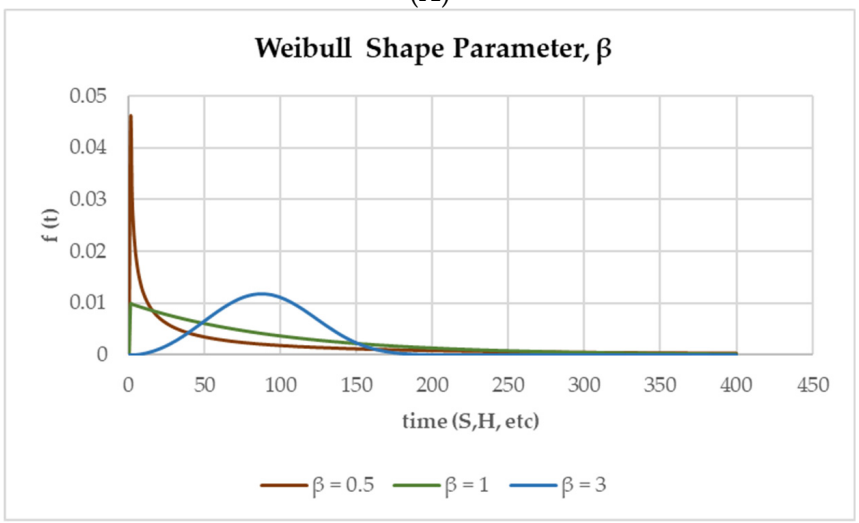

(**B**)

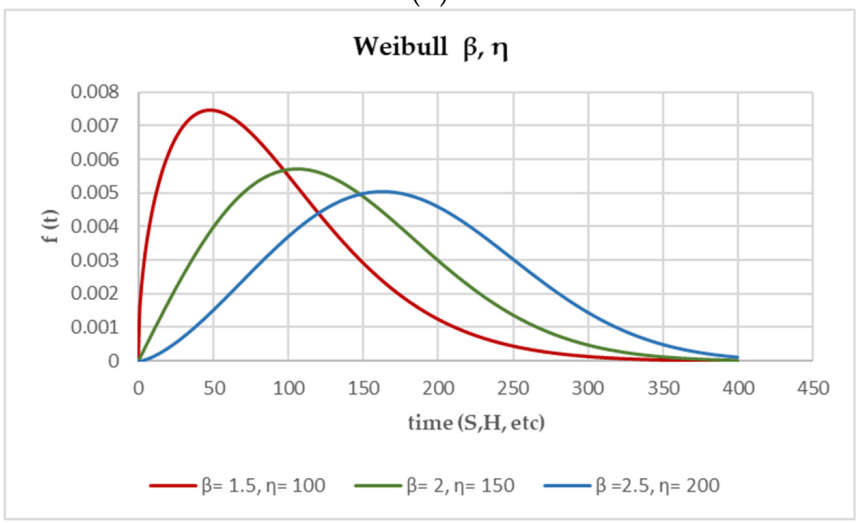

(**C**)

Figure 2. The relationship of probability density f(t) with shape and scale factors: (**A**) Effect of scale factor on probability. (**B**) Effect of shape factor on probability curve. (**C**) Frequency of shape and scale factors and their effect on probability function.

2.4. Time Series

Each natural environment does not have constant conditions. Marine environments develop and change in time under various parameters. Wind speed and direction and wind energy are changing in space and time, which may have a serious impact on cost efficiency in wind energy generation, and in worse cases may threaten investments in this energy sector. Thus, investigation of temporal variability and trends in wind power potential at different locations is of primary importance.

Mann–Kendall Trend Test

The Mann–Kendall trend test is a nonlinear index and the degree to which an individual parameter continuously increases or decreases, and its range is between +1 and −1 [48]. The positive value indicates that the trend is constantly increasing and the negative value shows that the trend has been steadily decreasing, while zero indicates the absence of the trend. The Mann–Kendall trend test is defined as the following Equation (5) [49]:

$$\begin{gathered} S = \sum_{i=1}^{n-1} \sum_{j=i+1}^{n} sign\ (x_i - x_j) \\ sign\ (x_i - x_j) = \begin{cases} 1\ if\ x_i - x_j < 0 \\ 0\ if\ x_i - x_j = 0 \\ -1\ if\ x_i - x_j > 0 \end{cases} \end{gathered} \tag{5}$$

where n is the series for a long time, and x_i and x_j are observations at time i and j. For the analysis of the wind power density in the Caspian Sea, we used 1×1 degree spatial resolution.

3. Results

3.1. Wind Data Accuracy Evaluation

The results of the correlation analysis between the measurement of wind speed derived from QuikSCAT and RapidSCAT satellites and the ERA-Interim atmospheric reanalysis are shown in Table 1 and Figure 3. It shows spatial and temporal variability of correlation between these datasets. Ruti et al. [50] showed that the total amount of data correlation offshore is increasing, as the impact of environmental factors on the characteristics of data and uncertainties is decreasing.

The outcomes of the correlation between remote sensing data sources and the numerical model are shown in Figure 3, Tables 1 and 2. The influence of environmental elements on the qualities and uncertainties of data is, however, generally diminishing as the quantity of data correlation offshore is rising. The highest correlations are observed in the Middle Caspian Sea for both datasets (0.83 for QuikSCAT and 0.67 for RapidSCAT). In general, the South Caspian has a correlation coefficient for the QuikSCAT of 0.75 and for the RapidSCAT of 0.35. These values correspond to those of [51], who conducted research on this particular region of the Caspian Sea. The lowest correlations are observed in the southeastern corner of the Southern Caspian and in the northeastern corner of the Northern Caspian.

Time variability of wind speed derived from ERA-Interim and QuikSCAT for 2000–2009 for the Northern, Middle and Southern Caspian, as well as for ERA-Interim and RapidSCAT for January 2014–November 2015 for the Middle and Southern Caspian, is presented in Figure 3. Figure 3 shows that in general, QuikSCAT data are larger than the ERA-Interim data in all three parts of the Caspian Sea. The minimal values of wind speed (observed during summer) coincide much better than the maximal values observed in wintertime, when a discrepancy between two datasets is much larger. Furthermore, it looks like a seasonal cycle in wind speed variability is much more pronounced in the Middle Caspian than in the Northern and Southern Caspian, where the cycle is modified. Figure 3 also shows that RapidSCAT data are, in general, larger than the ERA-Interim data.

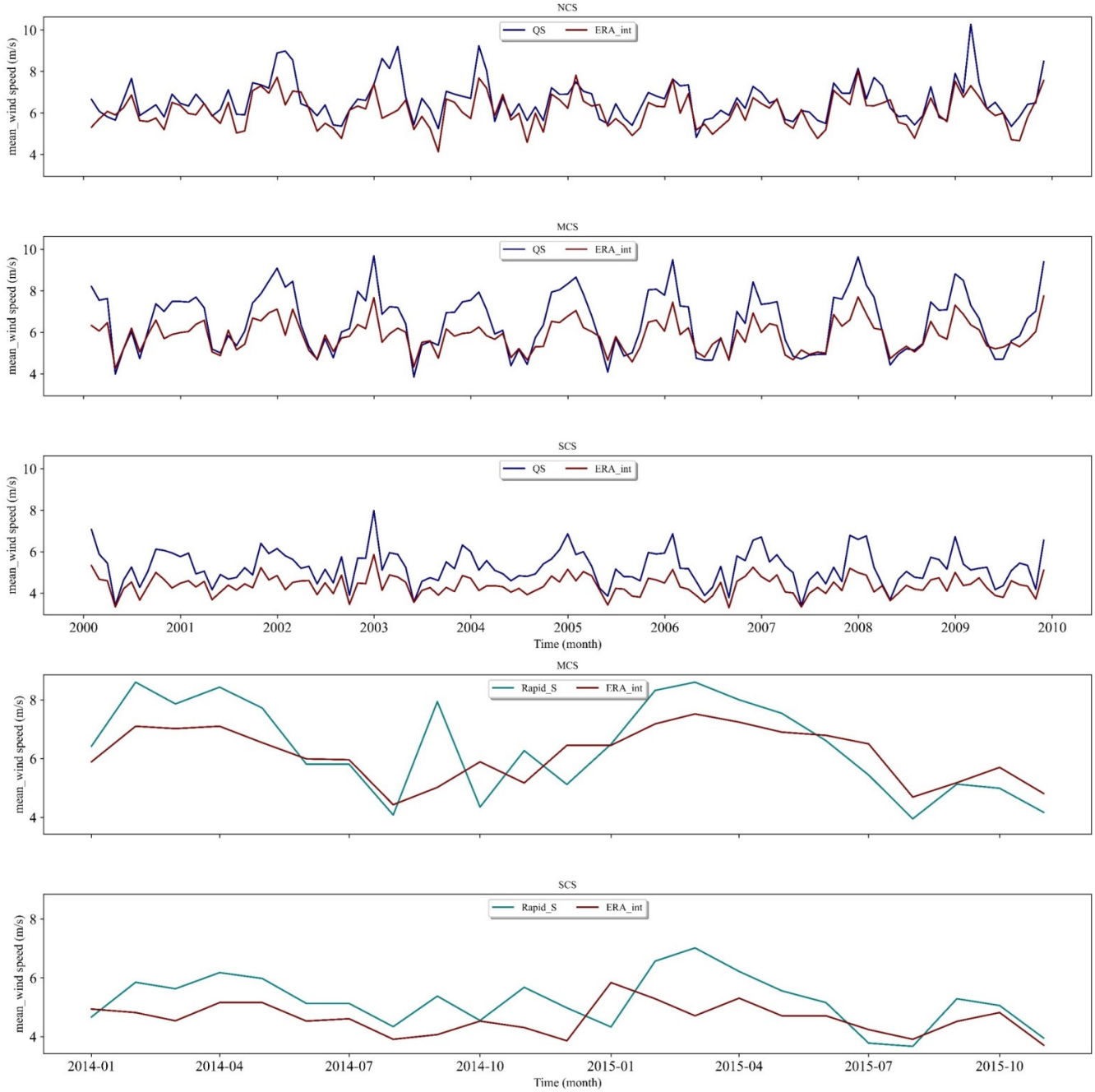

Figure 3. Time variability of wind speed (m/s): (NCS) Northern Caspian, 2000–2009, ERA-Interim and QuikSCAT; (MCS) Middle Caspian, 2000–2009, ERA-Interim and QuikSCAT; (SCS) Southern Caspian, 2000–2009, ERA-Interim and QuikSCAT; (MCS_RS) Middle Caspian, January 2014–November 2015, ERA-Interim and RapidSCAT; (SCS_RS) Southern Caspian, January 2014–November 2015, ERA-Interim and RapidSCAT.

Table 1 shows that the highest value of the RMSE for the QuikSCAT and RapidSCAT in the southern part of the Caspian Sea is 0.9 and 0.6, respectively, while the highest value of the correlation coefficient for the QuikSCAT and RapidSCAT is related to the Middle Caspian, which is as high as 0.93 and 0.76, respectively.

Table 1 shows that the higher the wind speed, the larger the difference between the QuikSCAT and ERA-Interim data. The highest correlation is observed in the Middle Caspian. The findings of [13] for the Brazilian coast are compatible with our results.

Table 1. Statistics for wind speed derived from the QuikSCAT and ERA-Interim data for the Northern, Middle, and Southern Caspian.

Part	Satellite	Mean (m/s)	SD (m/s)	MIN (m/s)	MAX (m/s)	CC (m/s)
Northern Caspian	QuikSCAT	5.26	0.48	3.08	8.93	0.75
	ERA-Interim	4.37	0.43	2.7	5.82	
Middle Caspian	QuikSCAT	6.56	0.6	4.29	8.85	0.83
	ERA-Interim	5.84	0.53	4.13	6.69	
Southern Caspian	QuikSCAT	6.45	0.6	0	10.35	0.59
	ERA-Interim	6.09	0.55	5.35	6.65	

The RapidSCAT data (Table 2) show lower correlation and a much larger difference with the ERA-Interim data, which needs to be investigated and explained in special research. The Middle Caspian has the greatest correlation coefficient value (0.67), while in the Southern Caspian it is of 0.37 only. Thus, the numerical model's data have a much better correlation with the QuikSCAT data.

Table 2. Statistics for wind speed derived from the RapidSCAT and ERA-Interim data for the Middle and Southern Caspian.

Part	Satellite	Mean (m/s)	SD (m/s)	MIN (m/s)	MAX (m/s)	CC (m/s)
Middle Caspian	RapidSCAT	6.41	1.54	3.97	7.52	0.67
	ERA-Interim	6.15	0.89	4.43	5.6	
Southern Caspian	RapidSCAT	5.22	0.85	3.67	7.2	0.37
	ERA-Interim	4.61	0.51	3.71	5.84	

3.2. Wind Speed and Indicators

Figure 4 shows an average wind speed over the Caspian Sea derived from ERA-Interim, QuikSCAT and RapidSCAT data for 1980–2016. The area of the Caspian Sea was divided by 67 boxes of 1 by 1 degree in the open sea and of different sizes in the coastal zone. We found that wind speed is more intense with increasing distance from the coast to offshore areas. In general, the western and southern parts of the Caspian Sea have a lower wind speed, as well as all narrow coastal regions. The Northern Caspian Sea seems to be the windiest region, the Middle Caspian has lower wind speed on average, and the Southern Caspian Sea is the calmest area of the Caspian Sea. Wind speed in boxes N64 (near the coast of Iran) and 15 (in the middle of the southern part of the Northern Caspian) are 1.84 and 6.20 m/s, respectively, with the lowest and the highest average values, which is consistent with the results obtained in [29]. The average wind speed for the entire Caspian Sea is 4.83 m/s. Therefore, we can conclude that the Caspian Sea wind regime is influenced by three main factors: peculiarities of regional atmospheric forcing, topography of the coasts (mountains, deserts, lowlands), and local wind flows affected by temperature differences between land and the sea.

Figure 5 shows seasonal variability of monthly mean wind speed for all 12 months of the year. The lowest seasonal variability is observed in the Southern Caspian Sea and the largest one is observed in the Northern Caspian Sea. Moreover, during the winter and spring seasons, we observe larger wind speed values than during summer and autumn.

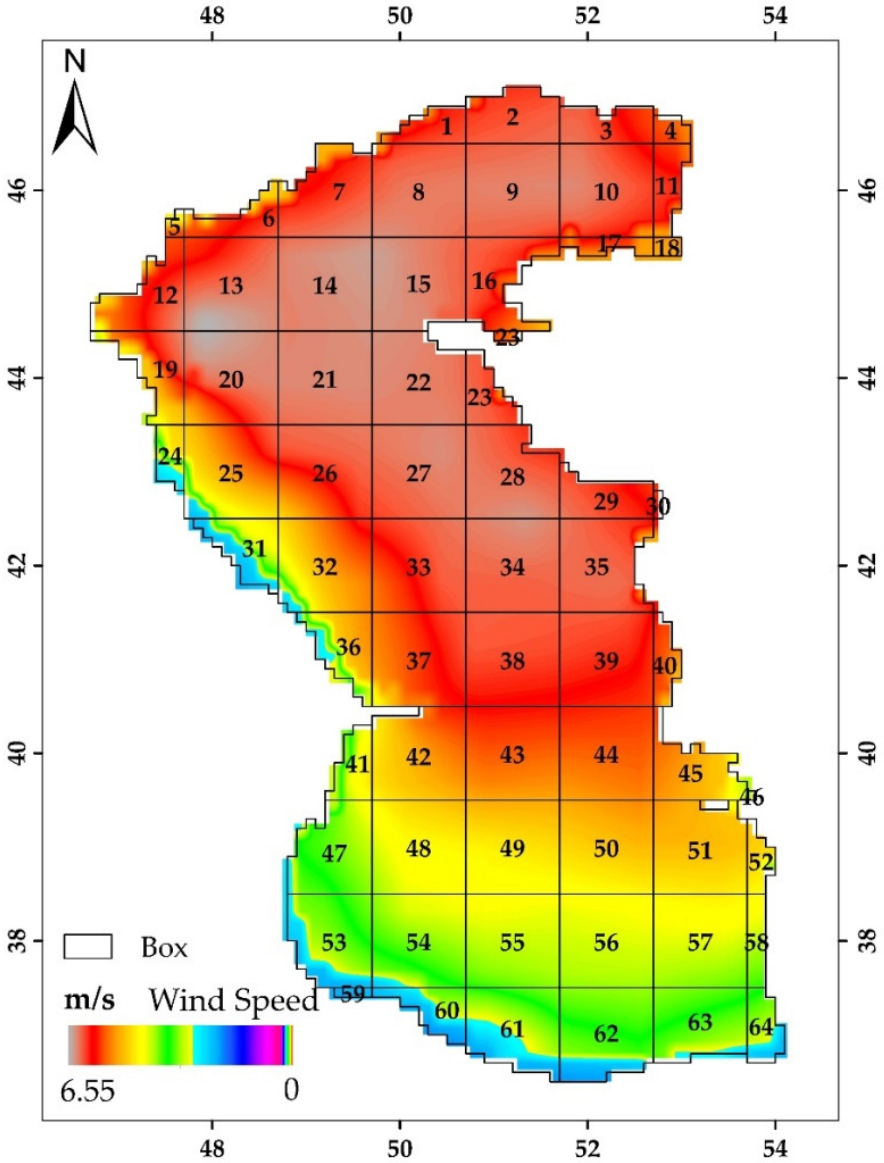

Figure 4. Average wind speed over the Caspian Sea over 37 years (1980–2015) based on the ERA-Interim, QuikSCAT, and RapidSCAT data.

The increase in winter wind speed is observed in all three parts of the sea. The highest wind speed for the Northern (6.7 m/s), Middle (6.3 m/s), and Southern (4.5 m/s) Caspian is observed in March (Figure 6). There is a decrease in wind speed from the end of spring (May) until late fall (October). September is the month with the lowest wind speed (4.9 m/s) for the Northern Caspian. July is the month with lowest wind speed for the Middle and Southern Caspian (Figure 6).

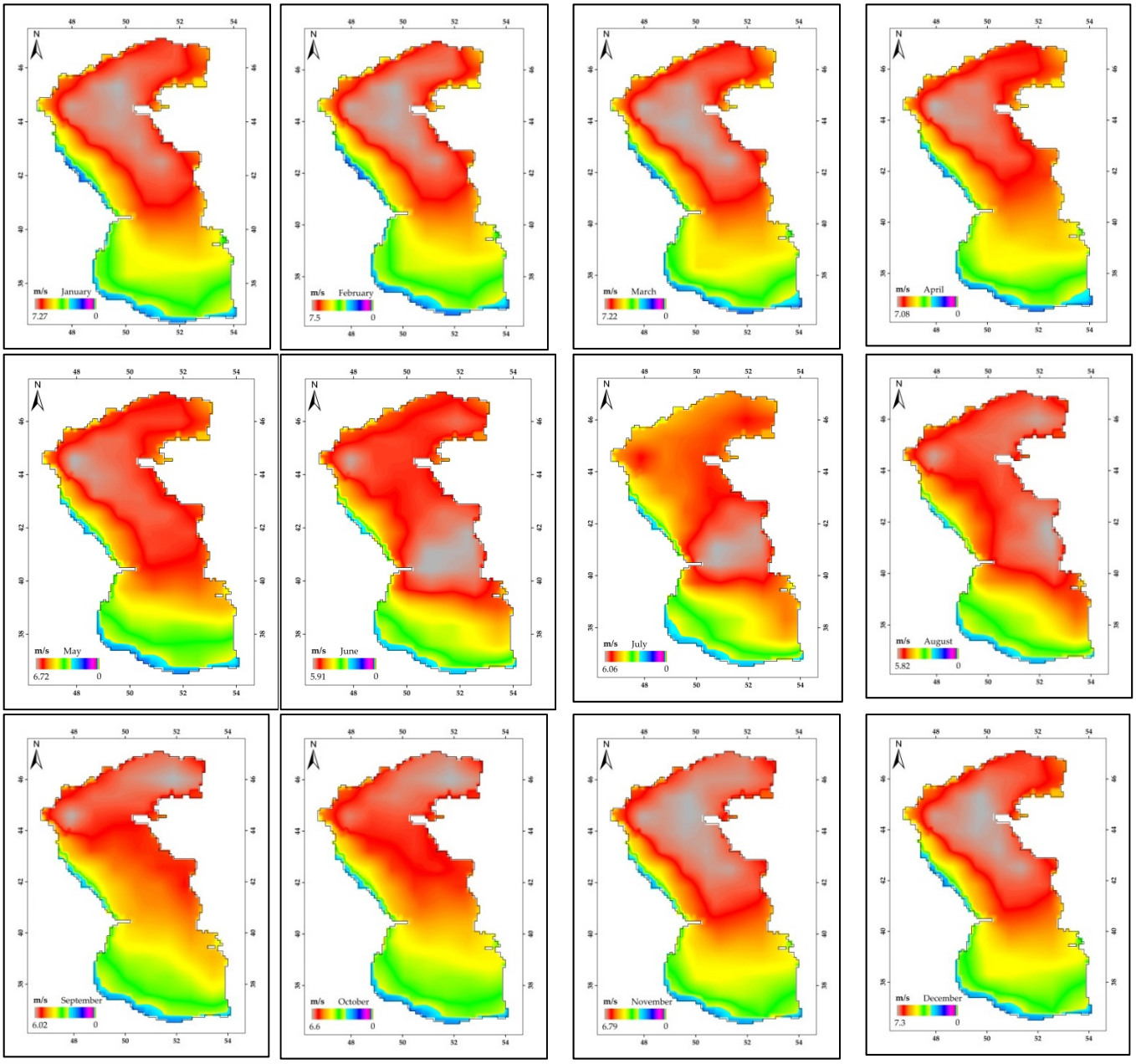

Figure 5. Seasonal (monthly) variability of an average wind speed over the Caspian Sea over 37 years (1980–2015) based on the ERA-Interim, QuikSCAT and RapidSCAT data.

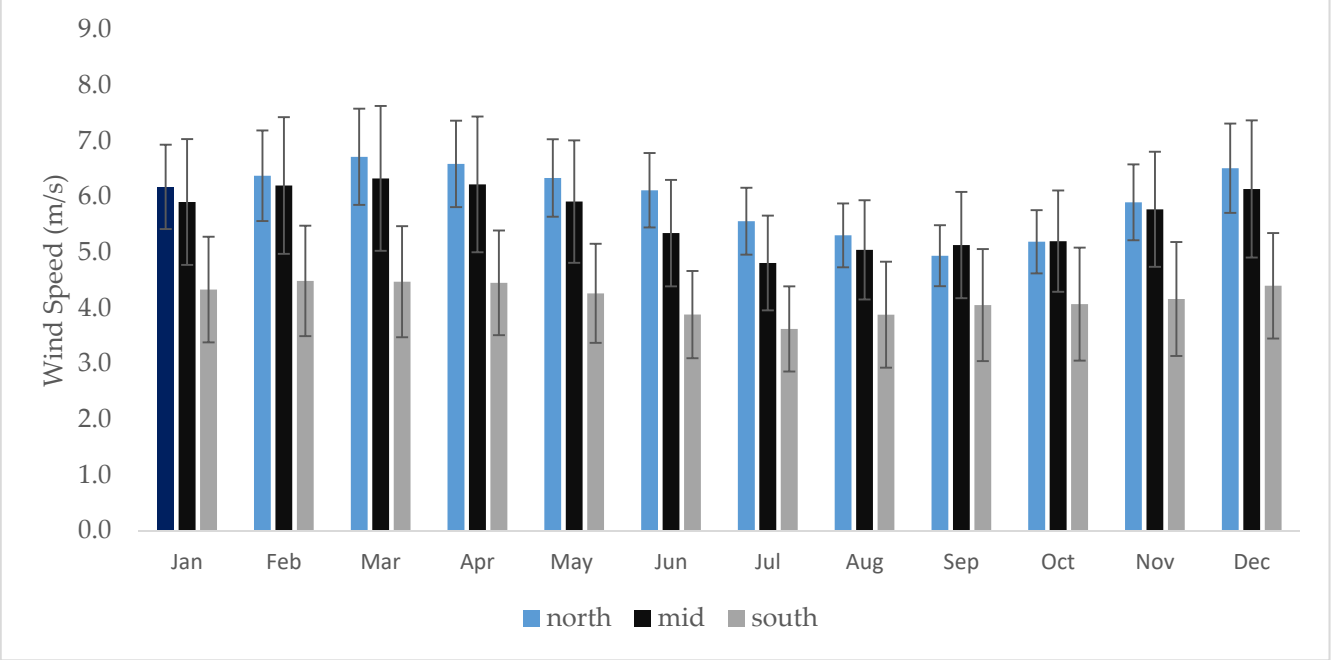

Figure 6. Monthly mean seasonal variations of wind speed (m/s) and standard deviation (m/s) in the Caspian Sea for 1980–2015.

3.3. Wind Power Density

The average power density for the entire Caspian Sea for 37 years (1980–2015) in Figure 7 shows that the overall average wind energy in the Caspian Sea is 173 W/m^2. This value shows a lower level of wind power in the Caspian Sea relative to other seas. The distribution of wind energy in the Caspian Sea is not homogeneous, it varies across the sea due to physicogeographical and meteorological peculiarities. This energy on the boundary between the Northern and Middle Caspian is much higher than in other parts of the Caspian Sea, and ranges between 250–300 W/m^2 (Figure 7). Wind power energy gradation better reflects spatial distribution of this wind parameter. The southern part of the Southern Caspian is characterized by the lowest values for the Caspian Sea (less than 100 W/m^2). The values of 200–250 W/m^2 are characteristic for the Middle and Northern Caspian, and this area is closer to the eastern coast than to the western one (Figure 7B).

Seasonal variations in wind power density in the Northern Caspian Sea for 1980–2015 show the highest values of 372 W/m^2, 356 W/m^2, 372 W/m^2, and 366 W/m^2 in 1987, 1989, 1993, and 1998, respectively (Figure 8). The maximum value of wind power density in the Northern Caspian was observed in winter of 1993 (130 W/m^2) and the minimum was observed in winter of 2003 (50.7 W/m^2). In spring, the maximum of 79.3 W/m^2 was recorded in 2000 and the minimum was recorded in 1986. In summer, the maximum of 65.9 W/m^2 was observed in 1998 and the minimum was recorded in 1999. In autumn, the maximum was 84.64 W/m^2 in 2001 and the minimum was recorded in 2000. The highest year-to-year fluctuations in the Northern Caspian Sea were recorded between 1998 and 2003.

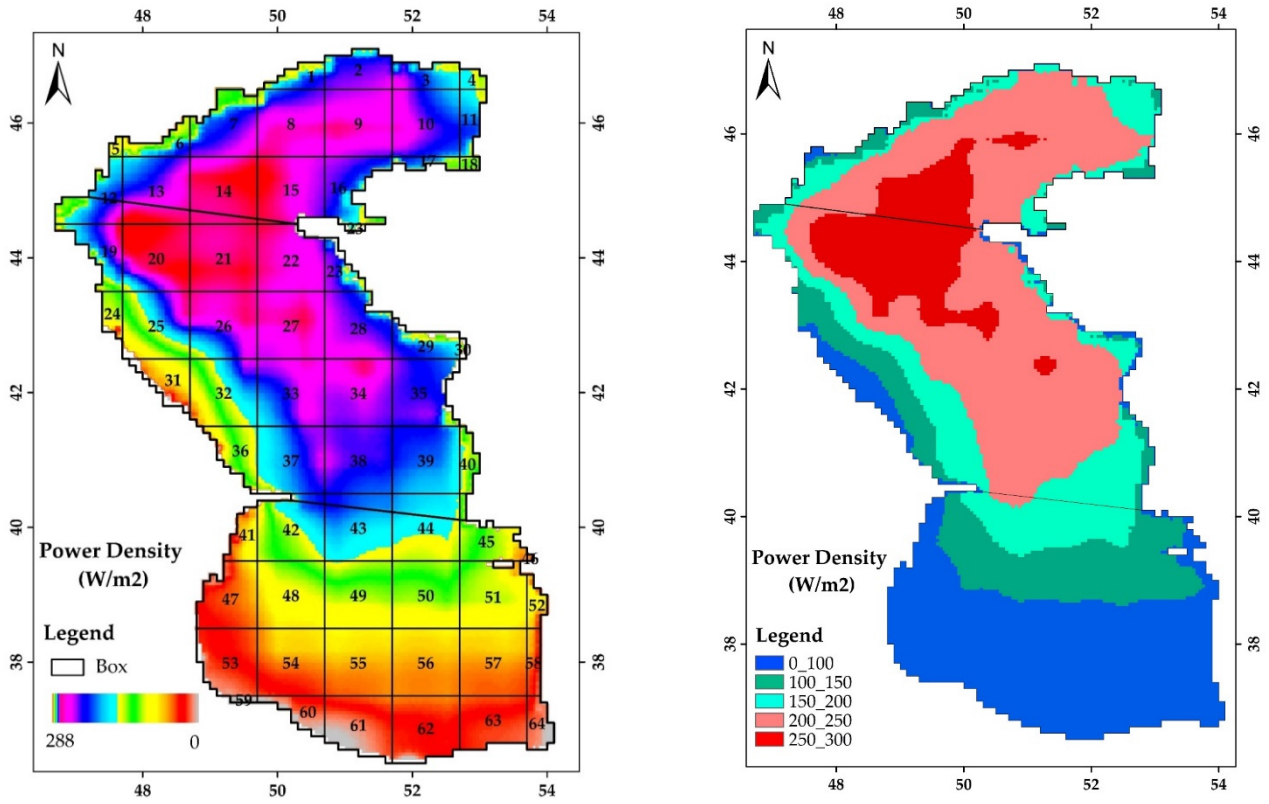

Figure 7. (**A**) Average wind power density (W/m^2) for 1980–2015; (**B**) Wind power density range gradation (W/m^2) for 1980–2015.

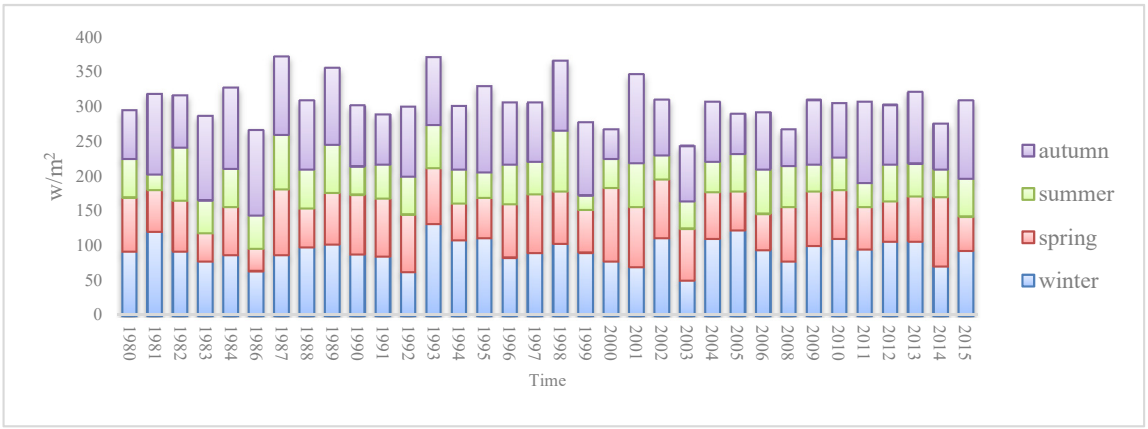

Figure 8. Seasonal variations in wind power density in the Northern Caspian Sea for 1980–2015. Winter—December, January, February; spring—March, April, May; summer—June, July, August; autumn—September, October, November.

Figure 9 shows seasonal variability in wind power density for the Middle Caspian Sea. The peak in winter wind energy of 130.4 W/m^2 was observed in 2010 and the minimum of 64.25 W/m^2 was observed in 2003. In spring, the maximum of 84.3 W/m^2 was recorded in 1990 and the minimum was observed in 1986 (40.5 W/m^2). In summer, the maximum of 82.3 W/m^2 was observed in 1997 and the minimum was observed in 1981 (33.4 W/m^2). In autumn, the maximum was 12.2 W/m^2 in 2015 and the minimum was observed in 2000 (54.9 W/m^2).

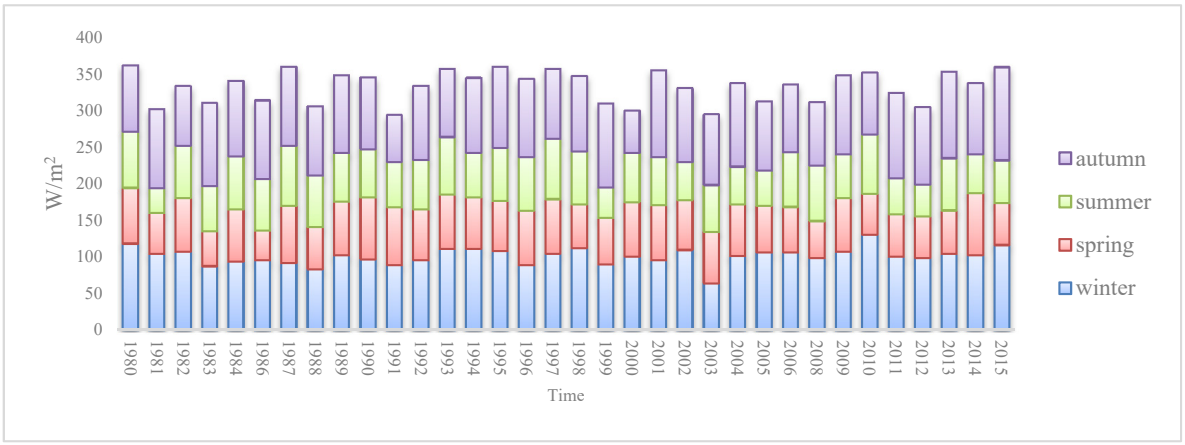

Figure 9. Seasonal variations in wind power density in the Middle Caspian Sea for 1980–2015.

Figure 10 depicts the Southern Caspian Sea's seasonal variations in wind power density. The peak power density was observed in the fall (61.65 W/m^2) and winter (46.25 W/m^2) seasons of 2002 and 1989, and then in the summer (33.23 W/m^2) and spring (28.8 W/m^2) seasons of 1997 and 2004, respectively. The minimum value of this variable was estimated in the fall season in 2010 (15.5 W/m^2), for the winter season in 1995 (12.8 W/m^2), and for the summer (8.6 W/m^2) and spring (6 W/m^2) seasons in 2005 and 1983, respectively.

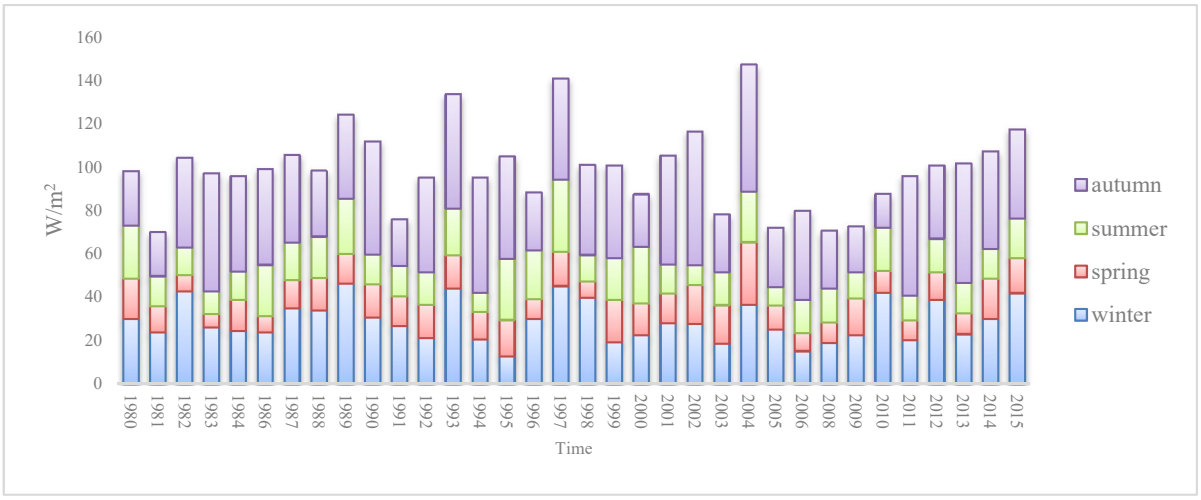

Figure 10. Seasonal variations in wind power density in the Southern Caspian Sea for 1980–2015.

3.4. Analysis of the Interannual Variability Trends

Figure 11 shows spatial variability in different interannual trends of wind speed and wind power. The results of wind velocity uniformity trends in the Caspian Sea (Figure 11A) show a wind speed decrease in the Northern Caspian Sea. The focus of this decrease is in boxes 2 and 9, but it is noteworthy that this trend is very low and reaches the average value in box 9 of −0.05 m/s in the time series. There is a dramatic increase in wind speed along the coasts of Iran. The focus of this trend is in boxes 59 (0.26 m/s), 60 (0.25 m/s), and 61 (0.29 m/s).

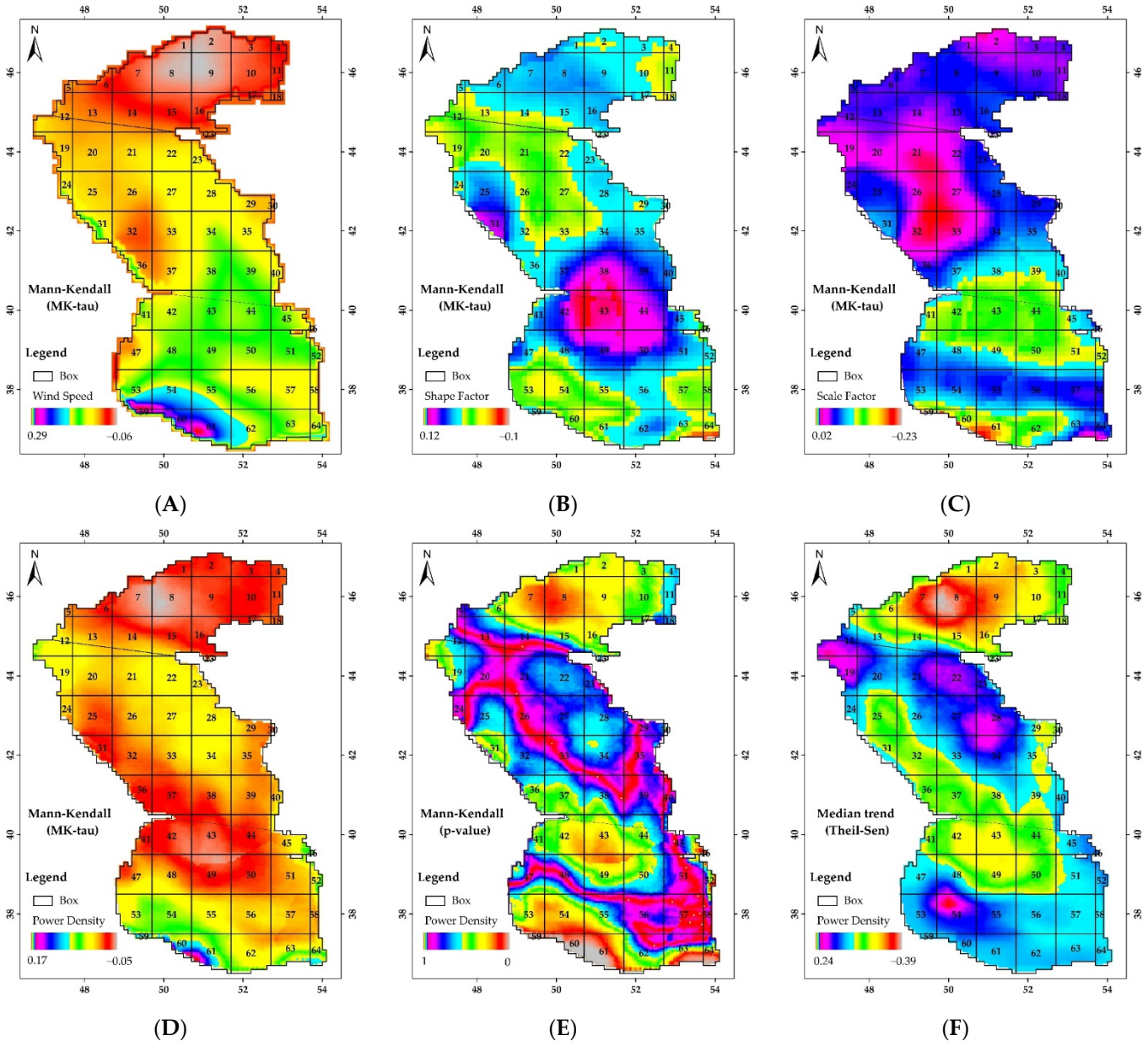

Figure 11. Mann–Kendall trend for wind speed (**A**), Mann–Kendall trend for shape factor (**B**), Mann–Kendall trend for scale factor (**C**), Mann–Kendall trend for power density (**D**), significant Mann–Kendall trend for wind power density (**E**), median trend for wind power density (**F**) for 1980–2015.

The results of the Mann–Kendall statistics show increasing and decreasing trends for both shape and scale factors in most of the regions of the Caspian Sea. Generally, for the shape factor (Figure 12B), boxes 64 (−0.1), 53 (−0.03) and 54 (−0.03) have the highest decreasing trends. In contrast, boxes 42, 43, and 38 have the highest rates of 0.129, 0.129, and 0.122, respectively. The shape factor represents spatial variability of wind speed; in other words, reduced wind speed variations and increased wind speed dependability result from an increase in the shape factor.

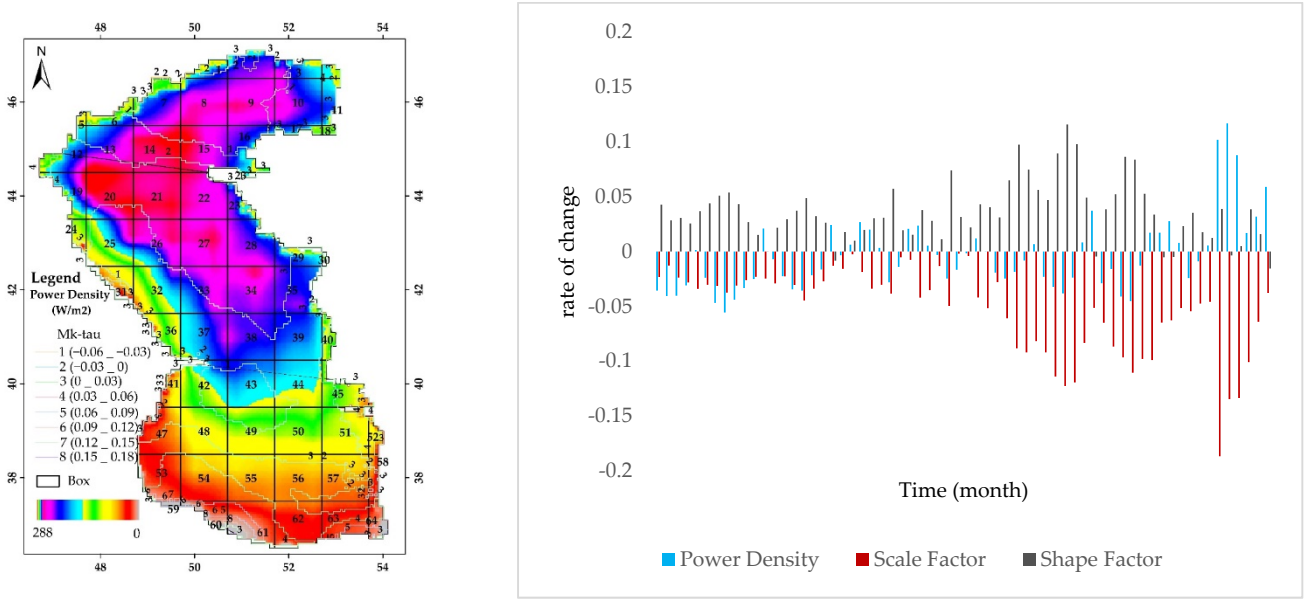

Figure 12. Wind power density and the trend of wind power density changes in the Caspian Sea (**A**); Changes in each profile's wind power density and scale and shape factors on a monthly basis from 1980 to 2015 (**B**).

For the scale factor (Figure 11C), boxes 59 (−0.238), 60 (−0.235), and 61 (−0.212) have the largest decreasing trends for the whole Caspian Sea, while boxes 32 and 33 have the highest rates of 0.02. The results of this section, according to the decreasing trend of the scale factor, indicate a general decrease in wind speed and a decrease in the probability according to Equations (3) and (4), which can also be adjusted according to the shape factor.

The power density (Figure 11D,E) shows the highest increasing rate of 0.172, 0.17, and 0.13 in the coastal zone of Iran, in boxes 61, 60, and 59, respectively. This is consistent with the Mann–Kendall statistics for wind speed in these boxes (Figure 11A). The highest decreasing Mk-trend in the power density of −0.05 is observed in the Northern Caspian (boxes 7 and 8), −0.03 (boxes 25 and 31) in the middle of the Caspian Sea, and of −0.04 in boxes 43 and 49 in the Southern Caspian. In general, in the Caspian Sea, power density has generally been decreasing. The Middle Caspian has experienced the largest decrease in the area (54.54%), followed by the Southern Caspian (52.7%) and the Northern Caspian (6.54%) (Figure 11D).

Spatial distribution for the significant Mann–Kendall trend for wind power density (Figure 11E) indicates that the *p*-value in boxes 62 and 63 is smaller than 0.05, which means a significance of trend with a confidence level of 95% [49].

Spatial distribution of a median trend in wind power (Figure 11F) shows a significant decrease in boxes 7, 8, and 9 in the Northern Caspian. A slightly lower rate of wind power decrease is observed in the northern part of the Southern Caspian. However, in general, the whole Caspian Sea has a negative trend of −0.5 W/m^2yr for the entire time period of 1980–2015. In the Southern Caspian, this rate was −0.24 W/m^2yr. Unlike the Northern and the Southern Caspian, the Middle Caspian has an increasing trend of 0.179 W/m^2yr on average. Here, the highest rates of 0.19, 0.17, and 0.166 are observed in boxes 19, 34, and 28, respectively. The total power loss rate in the Caspian Sea for 36 years is equal to 16.85 W/m^2, which is a very low drop relative to the average value of 173 W/m^2 characteristic for the Caspian Sea for these years.

4. Discussion

The Caspian Sea countries are rich in hydrocarbon resources. Iran, Azerbaijan, Russia, Kazakhstan, and Turkmenistan are producers and exporters of oil and gas from this

region [52]. This fact explains a low interest to wind energy (and other renewable energy) production, including both onshore and offshore wind energy. Nevertheless, such kinds of research on investigation of wind energy production potential should be carried out to assess general characteristics of this type of renewables, its interannual trends, and efficiency of wind farm construction, at least for local needs, due to remote locations and a lack of energy supply infrastructure for many areas around the Caspian Sea.

Planning of offshore wind farm construction requires exact information on spatial distribution of wind speed and wind power density and their interannual trends. For the Caspian Sea, this is a difficult task due to a lack of weather stations and wind speed observations at coastal weather stations and offshore. Partially this is explained by uninhabited deserts on the eastern coasts and steppes on the northern coasts of the sea [53]. This results in uncertainties in the atmospheric reanalysis data for this region, which can be decreased by the use of satellite remote sensing data, which have their own advantages and disadvantages. In the present study, we used both satellite and model datasets to overcome this problem.

We investigated the correlation between the QuikSCAT and RapidSCAT remote sensing data and ERA-Interim model data on wind speed for 1980–2015. Despite the good correlation between these datasets, the model data have better time and space resolution. The correlation for the Middle and Southern Caspian was significant at 0.93 and 0.92 on average. In contrast, the Northern Caspian shows lower correlation coefficients of 0.59, probably due to the physicogeographical, meteorological, and climatic peculiarities of the region [54].

Our results show that the Northern Caspian Sea is the windiest region, with a maximum average wind speed of 6.20 m/s in the middle of the southern part of the Northern Caspian. The Middle Caspian has a lower wind speed on average, and the Southern Caspian Sea is the calmest area of the Caspian Sea, with a minimum average value of 1.84 m/s near the coast of Iran. The average wind speed for the entire Caspian Sea is 4.83 m/s. This wind speed spatial distribution reflects a similar distribution of wind power density.

The average power density for the entire Caspian Sea over 37 years (1980–2015) was 173 W/m^2. This is at least three times less than the global mean wind power at 10 m (487 W/m^2) for 2000–2006 [12]. Onea and Rusu [30] and Rusu [26] showed that offshore wind farms can be efficient in the coastal environment of the Black Sea, where the maximum wind power at 100 m can reach 548 W/m^2. The distribution of wind energy in the Caspian Sea is not homogeneous; this energy on the boundary between the Northern and Middle Caspian is much higher than in other parts of the Caspian Sea, and ranges between 250–300 W/m^2. The values of 200–250 W/m^2 are characteristic for the Middle and Northern Caspian, and this area is closer to the eastern coast than to the western one. This is consistent with [33], who showed for 1999–2008 that the highest values of power density of up to 300 W/m^2 for the total time and up to 426 W/m^2 for wintertime were obtained for the coastal zone of Kazakhstan between Fort-Shevchenko and Aktau in the northeastern part of the Middle Caspian Sea.

As concerns the interannual variability of wind power, the spatial distribution of a median trend in wind power (Figure 11F) shows a significant decrease in the Northern Caspian, where we have the maximum of average wind power. In the Middle Caspian, there is an increasing trend of 0.178 W/m^2yr on average. In general, the whole Caspian Sea has a negative median trend of -0.5 W/m^2yr for the entire period of 1980–2015. This is not critical, because the total power loss rate in the Caspian Sea over 37 years is equal to 16.88 W/m^2, which is a very small drop relative to the average value of 173 W/m^2 characteristic for the Caspian Sea for these years.

Figure 12B shows a combination of average wind power density and its trends. For example, high energy density in the Northern Caspian is accompanied by a decreasing interannual trend with a maximum negative rate in box 8. In boxes 43, 42, and 49 (the Southern Caspian), there is also a decreasing trend that lies on the average power density

values of 100–200 W/m^2. We found that boxes 22 and 27 and surrounding areas in the eastern part of the Middle Caspian have relatively high average values of power density and the highest positive rates of interannual changes, which makes them ideal locations for future offshore wind farm development. Figure 12B can be practically used for assessment of different locations of the Caspian Sea for efficient production of wind energy.

5. Conclusions

The results of this study showed that two-thirds of the area of the Caspian Sea has a wind power of 200–300 W/m^2, which is a relatively high level for wind energy production (Figure 7B). This area is located in the Northern and Middle Caspian Sea and it is pressed against the eastern coast of the sea. As was already mentioned in [12], there is an increase in wind power from the shore to the shelf break. Figure 8 shows exactly this distribution of wind power along all coasts of the Caspian Sea, with some places in the Northern Caspian where there is a high gradient of wind power between the shore and offshore, when wind power can change from 0–50 W/m^2 to 250–300 W/m^2 at a short distance.

From the wind farm construction point of view, the Northern Caspian seems to be an ideal place because of the high level of wind power and shallow depths, which are on average 5–6 m. However, the main problem will be an ice cover, which is established yearly in the eastern part or the whole area of the Northern Caspian [55,56]. The ice cover is always in motion due to wind forcing, which sometimes leads to ice hummock formation (stamukhi). Stamukhi are usually so thick that they reach the bottom and can cut the bottom surface along several kilometers. Both features—moving ice fields and stamukhi—will represent a real danger to offshore wind turbines, bottom cables, and the substations. Recently, we have observed great interest in weathervaning technology for floating offshore wind turbines (FOWT), which can significantly increase the efficiency of offshore wind farms [57]. This refers to the ability of the entire floating structure (composed of a floater and a turbine) to be passively aligned along the wind direction so that the rotor is set perpendicular to the incoming wind direction. This is achieved by allowing the floating structure to rotate freely over the pivot point anchored at the bottom with which the floating structure is connected by a steel cable or chains. This sophisticated and very expensive construction will not help much in the ice conditions because the floater will be aligned along the direction of ice field movement, which is affected by currents as well. Steel cables and chains connecting the floater with the bottom anchor (pivot point) will not withstand the pressure of the ice field.

Thus, the Middle Caspian seems to be the best place for wind farm construction. Its average depth is of 190 m; this is why it can be suggested that the best place will be shallow coastal areas along the coast of Kazakhstan between Fort-Shevchenko (44°30′N) in the north to 42°00′N in the south, which is almost the border with Turkmenistan. This area displays positive interannual trends in wind power density, which is also an important factor for future wind energy generation. This place can be supported by the related infrastructure that can be established in the cities of Fort-Shevchenko and Aktau.

As concerns the other Caspian Sea countries, the coastal areas of Turkmenistan, Iran, Azerbaijan, and Dagestan in Russia are not prospective for offshore wind power generation due to low values of wind power density. The western coastal areas of Russia northward of 44°30′N are much more prospective, but this is the place where ice cover issues appear and a decreasing trend is observed. The solution of this problem is to investigate the onshore wind power generation along the coasts of the Caspian Sea, which is out of the scope of this paper but seems to be a logical continuation of the present research. In many coastal areas, topographic features generate local strong winds, which can be used for effective wind power generation.

Author Contributions: Conceptualization, all authors; methodology, M.R., M.G., B.A. and A.R.; software, M.R., M.G., B.A. and A.R.; validation, M.R., M.G. and A.R.; formal analysis, M.R., M.G., A.R. and A.G.K.; investigation, all authors; data curation, M.R., M.G. and A.R.; writing—original draft preparation, M.R., M.G. and A.R.; writing—review and editing, A.G.K. and A.V.S.; visualization,

M.R., M.G. and A.R.; funding acquisition, A.G.K. and A.V.S. All authors have read and agreed to the published version of the manuscript.

Funding: A.G.K. was partially supported in the framework of the P.P. Shirshov Institute of Oceanology RAS budgetary financing from Ministry of Science and Higher Education Project N FMWE-2021–0015 "Extreme hazards associated with the oceans".

Data Availability Statement: All freely available data are mentioned in Section Data and Methods.

Acknowledgments: The study presented here is part of the thesis in partial fulfillment of the requirements for the degree of M.Sc. of the first author at Tarbiat Modarres University (T.M.U.) of Iran; the authors extend their appreciation for the support provided by the authorities of Tarbiat Modares University in funding the study. Moreover, the research was conducted in the framework of the "The Caspian Sea Digital Twin" project endorsed by the IOC-UNESCO and performed as part of the activities related to the UN Decade of Ocean Science for Sustainable Development (2021–2030). The authors would like to thank *Remote Sensing*, MDPI, for coverage of the APC.

Conflicts of Interest: The authors declare no conflict of interest.

References

1. Barbier, E.B. Marine ecosystem services. *Curr. Biol.* **2017**, *27*, R507–R510. [CrossRef] [PubMed]
2. Busch, M.; Gee, K.; Burkhard, B.; Lange, M.; Stelljes, N. Conceptualizing the link between marine ecosystem services and human well-being: The case of offshore wind farming. *Int. J. Biodivers. Sci. Ecosyst. Serv. Manag.* **2011**, *7*, 190–203. [CrossRef]
3. Fisher, B.; Turner, R.K.; Morling, P. Defining and classifying ecosystem services for decision making. *Ecol. Econ.* **2009**, *68*, 643–653. [CrossRef]
4. Fisher, B.; Turner, R.K. Ecosystem services: Classification for valuation. *Biol. Conserv.* **2008**, *141*, 1167–1169. [CrossRef]
5. Lee, J.; Backwell, B.; Clarke, E.; Williams, R.; Liang, W.; Fang, E.; Ladwa, R.; Muchiri, W.; Fiestas, R.; Qiao, L.; et al. *Global Wind Report 2022*; GWEC: Brussels, Belgium, 2022; p. 158.
6. Mostafaeipour, A. Feasibility study of offshore wind turbine installation in Iran compared with the world. *Renew. Sustain. Energy Rev.* **2010**, *14*, 1722–1743. [CrossRef]
7. Rabbani, R.; Zeeshan, M. Exploring the suitability of MERRA-2 reanalysis data for wind energy estimation, analysis of wind characteristics and energy potential assessment for selected sites in Pakistan. *Renew. Energy* **2020**, *154*, 1240–1251. [CrossRef]
8. Olauson, J. ERA5: The new champion of wind power modelling? *Renew. Energy* **2018**, *126*, 322–331. [CrossRef]
9. Osinowo, A.A.; Lin, X.; Zhao, D.; Zheng, K. On the wind energy resource and its trend in the East China Sea. *J. Renew. Energy* **2017**, *2017*, 9643130. [CrossRef]
10. Cannon, D.J.; Brayshaw, D.J.; Methven, J.; Coker, P.J.; Lenaghan, D. Using reanalysis data to quantify extreme wind power generation statistics: A 33 year case study in Great Britain. *Renew. Energy* **2015**, *75*, 767–778. [CrossRef]
11. Kubik, M.; Brayshaw, D.J.; Coker, P.J.; Barlow, J.F. Exploring the role of reanalysis data in simulating regional wind generation variability over Northern Ireland. *Renew. Energy* **2013**, *57*, 558–561. [CrossRef]
12. Capps, S.B.; Zender, C.S. Estimated global ocean wind power potential from QuikSCAT observations, accounting for turbine characteristics and siting. *J. Geophys. Res. Atmos.* **2010**, *115*. [CrossRef]
13. Pimenta, F.; Kempton, W.; Garvine, R. Combining meteorological stations and satellite data to evaluate the offshore wind power resource of Southeastern Brazil. *Renew. Energy* **2008**, *33*, 2375–2387. [CrossRef]
14. Signell, R.P.; Carniel, S.; Cavaleri, L.; Chiggiato, J.; Doyle, J.D.; Pullen, J.; Sclavo, M. Assessment of wind quality for oceanographic modelling in semi-enclosed basins. *J. Mar. Syst.* **2005**, *53*, 217–233. [CrossRef]
15. Lebedev, S.A.; Kostianoy, A.G. Satellite altimetry of the Caspian Sea. *Sea Mosc.* **2005**, *366*, 113–120.
16. Lebedev, S.A.; Kostianoy, A.G. Integrated use of satellite altimetry in the investigation of the meteorological, hydrological, and hydrodynamic regime of the Caspian Sea. *TAO: Terr. Atmos. Ocean. Sci.* **2008**, *19*, 7. [CrossRef]
17. Zonn, I.S.; Kosarev, A.N.; Glantz, M.H.; Kostianoy, A.G. *The Caspian Sea Encyclopedia*; Springer: Berlin/Heidelberg, Germany, 2010.
18. Melnikov, V.; Zatsepin, A.; Kostianoy, A.G. *Hydrophysical Polygon on the Black Sea*; Russian State Oceanographic Institute: Moscow, Russia, 2011; Volume 213, pp. 264–278.
19. Hadadpour, S.; Moshfeghi, H.; Jabbari, E.; Kamranzad, B. Wave hindcasting in Anzali, Caspian Sea: A hybrid approach. *J. Coast. Res.* **2013**, *65*, 237–242. [CrossRef]
20. Grinevetsky, S.R.; Zonn, I.S.; Zhiltsov, S.S.; Kosarev, A.N.; Kostianoy, A.G. *The Black Sea Encyclopedia*; Springer: Berlin/Heidelberg, Germany, 2015.
21. Evstigneev, V.; Naumova, V.; Voskresenskaya, E.; Evstigneev, M.; Lyubarets, E. *Wind-Wave Conditions of the Coastal Zone of the Azov-Black Sea Region*; Institute of Natural and Technical Systems: Sevastopol, Crimea, 2017.
22. Kostianaia, E.A.; Serykh, I.V.; Kostianoy, A.G.; Lebedev, S.A.; Akhsalba, A.K. Climate Changes of the Wind Module in the Region of the Eastern Coast of the Black Sea. *Vestn. Tver State Univ. Ser. Geogr. Geoecol.* **2018**, *3*, 79–98.

23. Serykh, I.; Kostianoy, A. The links of climate change in the Caspian Sea to the Atlantic and Pacific Oceans. *Russ. Meteorol. Hydrol.* **2020**, *45*, 430–437. [CrossRef]
24. Kostianaia, E.A.; Kostianoy, A.G. Regional Climate Change Impact on Coastal Tourism: A Case Study for the Black Sea Coast of Russia. *Hydrology* **2021**, *8*, 133. [CrossRef]
25. Bogdanovich, Y.; Lipka, O.N.; Krylenko, M.V.; Andreeva, A.P.; Dobrolyubova, K.O. Climate threats in the North-West Caucasus Black Sea coast: Modern trends. *Fundam. Appl. Climatol.* **2021**, *7*, 44–70. [CrossRef]
26. Rusu, E. Wind climate scenarios in the Black Sea basin until the end of the 21st century. *Rom. J. Tech. Sciences. Appl. Mechanics.* **2021**, *66*, 181–204.
27. Manzano-Agugliaro, F.; Alcayde, A.; Montoya, F.G.; Zapata-Sierra, A.; Gil, C. Scientific production of renewable energies worldwide: An overview. *Renew. Sustain. Energy Rev.* **2013**, *18*, 134–143. [CrossRef]
28. Kerimov, R.; Ismailova, Z.; Rahmanov, N. Modeling of wind power producing in Caspian Sea conditions. *Int. J. Tech. Phys. Probl. Eng.* **2013**, *15*, 136–142.
29. Rusu, E.; Onea, F. Evaluation of the wind and wave energy along the Caspian Sea. *Energy* **2013**, *50*, 1–14. [CrossRef]
30. Onea, F.; Rusu, E. Wind energy assessments along the Black Sea basin. *Meteorol. Appl.* **2014**, *21*, 316–329. [CrossRef]
31. Onea, F.; Rusu, E. An evaluation of the wind energy in the North-West of the Black Sea. *Int. J. Green Energy* **2014**, *11*, 465–487. [CrossRef]
32. Rahmanov, N.; Kerimov, R.; Gurbanov, E. Assessing the wind potential of Caspian Sea region for covering demand in neighboring countries and reducing of carbon emission. In Proceedings of the 2nd International Symposium on Energy Challenges & Mechanics, Aberdeen, UK, 18–20 August 2014.
33. Onea, F.; Raileanu, A.; Rusu, E. Evaluation of the wind energy potential in the coastal environment of two enclosed seas. *Adv. Meteorol.* **2015**, *2015*, 808617. [CrossRef]
34. Amirinia, G.; Kamranzad, B.; Mafi, S. Wind and wave energy potential in southern Caspian Sea using uncertainty analysis. *Energy* **2017**, *120*, 332–345. [CrossRef]
35. Terziev, S.; Kosarev, A.; Kerimov, A. Hydrometeorology and hydrochemistry of seas. Vol. 6, the Caspian Sea, No. 1. Hydrometeorological Conditions. *Leningr. Gidrometeoizdat* **1992**, *6*, 358p. (In Russian)
36. Mazaheri, S.; Kamranzad, B.; Hajivalie, F. Modification of 32 years ECMWF wind field using QuikSCAT data for wave hindcasting in Iranian Seas. *J. Coast. Res.* **2013**, *65*, 344–349. [CrossRef]
37. Kamranzad, B.; Etemad-Shahidi, A.; Chegini, V.; Hadadpour, S. Assessment of CGCM 3.1 wind field in the Persian Gulf. *J. Coast. Res.* **2013**, *65*, 249–253. [CrossRef]
38. Kramer, H.J. QuikSCAT. Available online: https://www.eoportal.org/satellite-missions/quikscat#seawinds (accessed on 21 November 2022).
39. Hoffmann, L.; Spang, R. An assessment of tropopause characteristics of the ERA5 and ERA-Interim meteorological reanalyses. *Atmos. Chem. Phys.* **2022**, *22*, 4019–4046. [CrossRef]
40. Dee, D.P.; Uppala, S.M.; Simmons, A.J.; Berrisford, P.; Poli, P.; Kobayashi, S.; Andrae, U.; Balmaseda, M.; Balsamo, G.; Bauer, P. The ERA-Interim reanalysis: Configuration and performance of the data assimilation system. *Q. J. R. Meteorol. Soc.* **2011**, *137*, 553–597. [CrossRef]
41. Kalam Azad, A.; Golam Rasul, M.; Yusaf, T. Statistical Diagnosis of the Best Weibull Methods for Wind Power Assessment for Agricultural Applications. *Energies* **2014**, *7*, 3056–3085. [CrossRef]
42. Twidell, J.; Gaudiosi, G. *Offshore Wind Power*; Multi-Science Publishing Company: Brentwood, UK, 2009; Volume 425.
43. Lai, C.-D. Generalized Weibull Distributions. In *Generalized Weibull Distributions*; Springer: Berlin/Heidelberg, Germany, 2014; pp. 23–75.
44. Bidaoui, H.; El Abbassi, I.; El Bouardi, A.; Darcherif, A. Wind speed data analysis using Weibull and Rayleigh distribution functions, case study: Five cities northern Morocco. *Procedia Manuf.* **2019**, *32*, 786–793. [CrossRef]
45. Pishgar-Komleh, S.; Keyhani, A.; Sefeedpari, P. Wind speed and power density analysis based on Weibull and Rayleigh distributions (a case study: Firouzkooh county of Iran). *Renew. Sustain. Energy Rev.* **2015**, *42*, 313–322. [CrossRef]
46. Kollu, R.; Rayapudi, S.R.; Narasimham, S.; Pakkurthi, K.M. Mixture probability distribution functions to model wind speed distributions. *Int. J. Energy Environ. Eng.* **2012**, *3*, 1–10. [CrossRef]
47. Pal, M.; Ali, M.M.; Woo, J. Exponentiated weibull distribution. *Statistica* **2006**, *66*, 139–147.
48. Ahmadi, B.; Gholamalifard, M.; Kutser, T.; Vignudelli, S.; Kostianoy, A. Spatio-Temporal Variability in Bio-Optical Properties of the Southern Caspian Sea: A Historic Analysis of Ocean Color Data. *Remote Sens.* **2020**, *12*, 3975. [CrossRef]
49. Neeti, N.; Eastman, J.R. A contextual mann-kendall approach for the assessment of trend significance in image time series. *Trans. GIS* **2011**, *15*, 599–611. [CrossRef]
50. Ruti, P.M.; Marullo, S.; d'Ortenzio, F.; Tremant, M. Comparison of analyzed and measured wind speeds in the perspective of oceanic simulations over the Mediterranean basin: Analyses, QuikSCAT and buoy data. *J. Mar. Syst.* **2008**, *70*, 33–48. [CrossRef]
51. Golshani, A.A.; Taebi, S. Evaluation of wind vectors observed by quikscat/seawinds using synoptic and atmospheric models data in iranian adjacant seas. *J. Mar. Eng.* **2009**, *4*, 47–63.
52. Zhiltsov, S.S.; Zonn, I.S.; Kostianoy, A.G.; Semenov, A.V. *The Caspian Sea Region. Subjects of the Caspian Littoral Countries: Geography, Resources, Economics*; Witte Moscow University: Moscow, Russia, 2019; Volume 3, 200p.

53. Zonn, I.S.; Kostianoy, A.G.; Zhiltsov, S.S.; Semenov, A.V. *The Caspian Sea Region. The Caspian Sea and the History of Its Exploration*; Witte Moscow University: Moscow, Russia, 2019; Volume 2, 312p.
54. Fore, A.G.; Stiles, B.W.; Chau, A.H.; Williams, B.A.; Dunbar, R.S.; Rodríguez, E. Point-wise wind retrieval and ambiguity removal improvements for the QuikSCAT climatological data set. *IEEE Trans. Geosci. Remote Sens.* **2013**, *52*, 51–59. [CrossRef]
55. Lavrova, O.Y.; Ginzburg, A.I.; Kostianoy, A.G.; Bocharova, T.Y. Interannual variability of ice cover in the Caspian Sea. *J. Hydrol.* **2022**, *17*, 100145. [CrossRef]
56. Lavrova, O.Y.; Kostianoy, A.G.; Mityagina, M.I.; Strochkov, A.Y.; Bocharova, T.Y. Remote sensing of sea ice in the Caspian Sea. In Proceedings of the Remote Sensing of the Ocean, Sea Ice, Coastal Waters, and Large Water Regions, Strasbourg, France, 9–12 September 2019; pp. 193–204.
57. González, J.S.; Payán, M.B.; Santos, J.M.R.; Rodríguez, Á.G.G. Optimal Micro-Siting of Weathervaning Floating Wind Turbines. *Energies* **2021**, *14*, 886. [CrossRef]